

Tests of Lorentz violation in $\bar{\nu}_\mu \rightarrow \bar{\nu}_e$ oscillations

L.B. Auerbach¹⁰, R.L. Burman⁷, D.O. Caldwell⁴, E.D. Church², A.K. Cochran⁹, J.B. Donahue^{7,*},
A.R. Fazely⁹, G.T. Garvey⁷, R. Gunasingha⁹, R.L. Imlay⁸, T. Katori⁶, W.C. Louis⁷,
K.L. McIlhany², W.J. Metcalf⁸, G.B. Mills⁷, V.D. Sandberg⁷, D. Smith⁵, I. Stancu¹
W.H. Strossman², R. Tayloe⁶, M. Sung⁸, W. Vernon³, D.H. White⁷, and S. Yellin⁴

(LSND collaboration)

¹University of Alabama, Tuscaloosa, Alabama, 35487

²University of California, Riverside, California 92521

³University of California, San Diego, California 92093

⁴University of California, Santa Barbara, California 93106

⁵Embry Riddle University, Prescott, Arizona 86301

⁶Indiana University, Bloomington, Indiana 47405

⁷Los Alamos National Laboratory, Los Alamos, New Mexico 87545

⁸Louisiana State University, Baton Rouge, Louisiana 70803

⁹Southern University, Baton Rouge, Louisiana 70813

¹⁰Temple University, Philadelphia, Pennsylvania 19122

(Dated: August 4, 2018)

A recently developed Standard-Model Extension (SME) formalism for neutrino oscillations that includes Lorentz and CPT violation is used to analyze the sidereal time variation of the neutrino event excess measured by the Liquid Scintillator Neutrino Detector (LSND) experiment. The LSND experiment, performed at Los Alamos National Laboratory, observed an excess, consistent with neutrino oscillations, of $\bar{\nu}_e$ in a beam of $\bar{\nu}_\mu$. It is determined that the LSND oscillation signal is consistent with no sidereal variation. However, there are several combinations of SME coefficients that describe the LSND data; both with and without sidereal variations. The scale of Lorentz and CPT violation extracted from the LSND data is of order 10^{-19} GeV for the SME coefficients a_L and $E \times c_L$. This solution for Lorentz and CPT violating neutrino oscillations may be tested by other short baseline neutrino oscillation experiments, such as the MiniBooNE experiment.

PACS numbers: 11.30.Cp, 14.60.Pq, 14.60.St

I. INTRODUCTION

Lorentz symmetry is one of the most fundamental ideas of both relativistic local quantum field theory and general relativity. Early tests, such as the Michelson-Morley and Kennedy-Thorndike experiments have established that Lorentz symmetry is an exact symmetry of nature. So it is natural to assume that Lorentz symmetry is an exact symmetry in the standard model (SM) of particle physics. However, since the SM does not address gravity, a fundamental theory of Planck-scale physics ($M_P \sim 10^{19}$ GeV), including string theory [1] and quantum gravity [2], may violate Lorentz and CPT symmetry [3].

If limited to conventional relativistic quantum mechanics, it is possible to establish a self-consistent low-energy effective theory with Lorentz and CPT violation; this is called the standard-model Extension (SME) [4]. The minimal-SME formalism has all the conventional properties of the standard model including observer Lorentz covariance, power counting renormalizability, energy momentum conservation, quantized field, micro causality, and spin-statistics with particle Lorentz and CPT violation due to background Lorentz tensor fields of the uni-

verse. The minimal SME also has $SU(3)_C \times SU(2)_L \times U(1)_Y$ gauge invariance. Since the background Lorentz tensor fields are fixed in spacetime, by definition, they do not transform under an active transformation law. That implies rotation and boost dependence of physics in a specific frame. This formalism focuses on the inverse Planck-scale effect which is believed to be suppressed by at least one order of the inverse Planck mass ($\sim \frac{E}{M_P}$, where E is the energy scale of the system under consideration). Therefore, the physics quantities involved in the formalism are perturbative.

Surprisingly, atomic physics has achieved this sensitivity level, and extensive experimental studies have been done (see, for example, Ref. [3]). A recent experiment [5] of this type reaches a sensitivity to a specific combination of SME coefficients to order $\sim 10^{-32}$ GeV, well beyond a basic estimate of the scale of new physics. In addition, spectral polarimetry of distant cosmological sources yields a similar sensitivity for another combination of SME coefficients [6]. However, many of the SME coefficients still have no experimental bounds.

Similarly, quantum interference experiments, such as meson oscillations, are also sensitive to the small effect of Lorentz and CPT violation [7]. Tests have been made using data from many experiments, including KTeV [8], FOCUS [9], BaBar [10], BELLE [11], and OPAL [12]. Recently, the SME formalism for neutrino oscillations,

*Deceased

another type of quantum interference experiment, has become available [13].

II. THE LSND EVIDENCE FOR NEUTRINO OSCILLATIONS

The Liquid Scintillator Neutrino Detector (LSND) experiment [14], completed at the Los Alamos National Laboratory (LANL), observed an excess of $\bar{\nu}_e$ in a beam of $\bar{\nu}_\mu$ created from μ^+ decay at rest. The data analysis used the sample of detected $\bar{\nu}_e p \rightarrow e^+ n$ events with positron energy $20 < E_{e^+} < 60$ MeV. If interpreted as $\bar{\nu}_\mu$ to $\bar{\nu}_e$ oscillations, this $\bar{\nu}_e$ excess implies a two-neutrino oscillation probability of $(0.264 \pm 0.067 \pm 0.045)\%$. Here the first error is statistical and the second error is systematic (neutrino flux, particle detection efficiency, cross sections, etc.). Despite the evidence for neutrino oscillations from solar neutrinos [15, 16, 17, 18, 19, 20], atmospheric neutrinos [21, 22], accelerator neutrinos [23], and reactor neutrinos [24], the oscillation signal observed at LSND remains a puzzle. Since the neutrino sector is thought as likely to reveal new physics, the LSND anomaly is often explained with new ideas such as a mass-difference CPT-violating model (see, for example Ref. [25]) or sterile neutrino models (see Ref. [26] for a recent example). The MiniBooNE experiment [27] at Fermilab is currently taking data to test the LSND signal.

III. LORENTZ VIOLATING NEUTRINO OSCILLATIONS

Perhaps LSND is seeing the first signal of Planck-scale physics [28]. To describe neutrino oscillations, including Lorentz and CPT violation, a recently developed formalism for neutrino oscillations [13, 29] using the SME framework [4] is employed. This framework allows for a sidereal time variation of the neutrino oscillation probability.

Within the SME framework, the neutrino free field Lagrangian becomes,

$$\mathcal{L} = \frac{1}{2} i \bar{\psi}_A \Gamma_{AB}^\mu \overleftrightarrow{D}_\mu \psi_B - \bar{\psi}_A M_{AB} \psi_B, \quad (1)$$

$$\Gamma_{AB}^\mu = \gamma^\mu \delta_{AB} + c_{AB}^{\mu\nu} \gamma_\nu + d_{AB}^{\mu\nu} \gamma_5 \gamma_\nu + e_{AB}^\mu + i f_{AB}^\mu \gamma_5 + \frac{1}{2} g_{AB}^{\mu\nu\lambda} \sigma_{\nu\lambda}, \quad (2)$$

$$M_{AB} = m_{AB} + i m_{5AB} \gamma_5 + a_{AB}^\mu \gamma_\mu + b_{AB}^\mu \gamma_5 \gamma_\mu + \frac{1}{2} H_{AB}^{\mu\nu} \sigma_{\mu\nu}. \quad (3)$$

The first term of Γ_{AB}^μ and the first and second terms of M_{AB} are the only nonzero terms in the case of conventional neutrino oscillations. The remaining terms in this Lagrangian represent the physics of the background fields. In general, the background Lorentz tensor fields are an infinite series, but if the focus is on a low-energy effective theory, these eight additional fields are complete.

Here, vacuum expectation values that contain $c_{AB}^{\mu\nu}$, $d_{AB}^{\mu\nu}$, and $H_{AB}^{\mu\nu}$ are CPT-even terms while e_{AB}^μ , f_{AB}^μ , $g_{AB}^{\mu\nu\lambda}$, a_{AB}^μ , and b_{AB}^μ are CPT-odd by definition of the background fields. Notice that each background field has flavor indices (A and B) that, unlike other systems, bring additional complication for the neutrino sector.

This Lagrangian leads to the modified Dirac equation,

$$(i \Gamma_{AB}^\mu \partial_\mu - M_{AB}) \psi_B = 0. \quad (4)$$

After some manipulation, this yields the effective Hamiltonian for active neutrino oscillations [13]. In particular, the effective Hamiltonian for active antineutrino to antineutrino oscillations is,

$$(h_{\text{eff}})_{ab} = |\vec{p}| \delta_{ab} + \frac{(\tilde{m}^2)_{ab}^*}{2|\vec{p}|} + \frac{1}{|\vec{p}|} [-(a_L)^\mu p_\mu - (c_L)^{\mu\nu} p_\mu p_\nu]_{ab}^*. \quad (5)$$

Here, the effective Hamiltonian is a 3×3 flavor Majorana basis matrix of three active, right-handed, antineutrinos. The original effective Hamiltonian [13] can describe $\nu - \nu$, $\bar{\nu} - \bar{\nu}$, and $\nu - \bar{\nu}$ oscillations, but, in this work, lepton-number violating $\nu - \bar{\nu}$ oscillations are not considered. Therefore, the neutrino and antineutrino sectors can be diagonalized separately. There is some coupling of SME coefficients, $(a_L)_{ab}^\mu = (a)_{ab}^\mu + (b)_{ab}^\mu$ and $(c_L)_{ab}^{\mu\nu} = (c)_{ab}^{\mu\nu} + (d)_{ab}^{\mu\nu}$. Also, other types of SME coefficients do not show up in this analysis. For the usual conventional neutrino oscillation case, the effective Hamiltonian (Eq. 5) contains only the first two terms. Then, the neutrino oscillation probability depends on Δm^2 and the mixing matrix. But, in this general form, including possible Lorentz and CPT violation, the diagonalization of the effective Hamiltonian is more complicated and, in general, it can not be represented by Δm^2 and the mixing matrix alone.

IV. THE SHORT-BASELINE APPROXIMATION

If the baseline of the neutrino beam is short compared with the neutrino oscillation length, L , the neutrino oscillation probability can be expanded with an effective Hamiltonian. Expressed to leading order in h_{eff} [29],

$$P_{\bar{\nu}_\mu \rightarrow \bar{\nu}_e} \simeq \frac{|(h_{\text{eff}})_{e\bar{\mu}}|^2 L^2}{(\hbar c)^2}. \quad (6)$$

Note that in this equation, unlike the equations above, \hbar and c have been explicitly included. Since, in the effective Hamiltonian, p^μ contains information about the propagation direction of the neutrino, this oscillation probability depends on the neutrino propagation direction. In order to form a phenomenological expression for the neutrino oscillation probability, it is most convenient to use a coordinate system fixed to the experiment [6, 30].

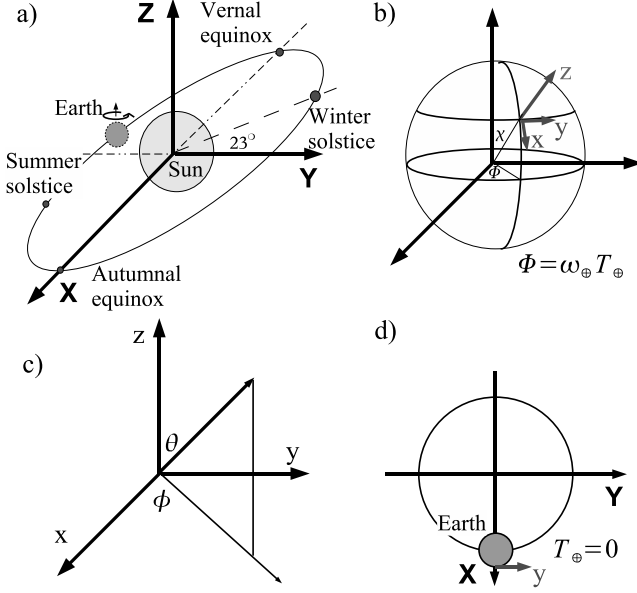


FIG. 1: Coordinate systems for the sidereal time variation analysis: a) the Sun-centered system, b) the Earth-centered system, c) the LANL local coordinate system, and d) the definition of $T_{\oplus} = 0$.

The standard choice is a Sun-centered system (Fig.1a) that is, to a good approximation, an inertial frame for the experiment.

With this choice of coordinates, the neutrino oscillation probability becomes,

$$P_{\nu_{\mu} \rightarrow \nu_e} \simeq \frac{L^2}{(\hbar c)^2} |(\mathcal{C})_{\bar{e}\bar{\mu}} + (\mathcal{A}_s)_{\bar{e}\bar{\mu}} \sin \omega_{\oplus} T_{\oplus} + (\mathcal{A}_c)_{\bar{e}\bar{\mu}} \cos \omega_{\oplus} T_{\oplus} + (\mathcal{B}_s)_{\bar{e}\bar{\mu}} \sin 2\omega_{\oplus} T_{\oplus} + (\mathcal{B}_c)_{\bar{e}\bar{\mu}} \cos 2\omega_{\oplus} T_{\oplus}|^2, \quad (7)$$

where ω_{\oplus} is the sidereal frequency ($=2\pi/23\text{h } 56\text{min } 4.1\text{s}$) and T_{\oplus} is the sidereal time as measured from a standard origin. Note that $P_{\nu_{\mu} \rightarrow \nu_e}$ may depend on the sidereal time.

These parameters, $(\mathcal{C})_{\bar{e}\bar{\mu}}$, $(\mathcal{A}_s)_{\bar{e}\bar{\mu}}$, $(\mathcal{A}_c)_{\bar{e}\bar{\mu}}$, $(\mathcal{B}_s)_{\bar{e}\bar{\mu}}$, and $(\mathcal{B}_c)_{\bar{e}\bar{\mu}}$, depend on the SME coefficients $(a_L)^\mu$ and $(c_L)^{\mu\nu}$ and the neutrino propagation direction unit vectors \hat{N}^X , \hat{N}^Y , and \hat{N}^Z in the Sun-centered system. The direction unit vectors depend on the colatitude χ of the experiment in the Earth-centered system (Fig.1b) and the zenith and azimuthal angles θ and ϕ of the $\bar{\nu}_{\mu}$ beam in the experiment local coordinate system (Fig.1c).

$$\begin{pmatrix} \hat{N}^X \\ \hat{N}^Y \\ \hat{N}^Z \end{pmatrix} = \begin{pmatrix} \cos \chi \sin \theta \cos \phi + \sin \chi \cos \theta \\ \sin \theta \sin \phi \\ -\sin \chi \sin \theta \cos \phi + \cos \chi \cos \theta \end{pmatrix} \quad (8)$$

For neutrinos from the Los Alamos Neutron Science Center (LANSCE) beam to the LSND detector, $\chi =$

54.1° , $\theta = 99.0^\circ$ and $\phi = 82.6^\circ$ [31]. The sidereal time is defined to be zero ($T_{\oplus} = 0$) at LANL local midnight on the autumnal equinox (Fig.1d). At that time, the y axis of the Earth-centered system coincides with the Y axis of the Sun-centered system. The estimated error using this definition is three minutes, which is small compared to the time scale sensitivity of this analysis.

Combining these values for neutrino propagation unit vectors with the detailed expression of the parameters, $(\mathcal{C})_{\bar{e}\bar{\mu}}$, $(\mathcal{A}_s)_{\bar{e}\bar{\mu}}$, $(\mathcal{A}_c)_{\bar{e}\bar{\mu}}$, $(\mathcal{B}_s)_{\bar{e}\bar{\mu}}$, and $(\mathcal{B}_c)_{\bar{e}\bar{\mu}}$ [29], yields, for the particular case of the LSND experiment:

$$(\mathcal{C})_{\bar{e}\bar{\mu}} = \frac{(\tilde{m}^2)_{\bar{e}\bar{\mu}}}{2E} + [(a_L)_{\bar{e}\bar{\mu}}^T + 0.19(a_L)_{\bar{e}\bar{\mu}}^Z] + E[-1.48(c_L)_{\bar{e}\bar{\mu}}^{TT} - 0.39(c_L)_{\bar{e}\bar{\mu}}^{TZ} + 0.44(c_L)_{\bar{e}\bar{\mu}}^{ZZ}], \quad (9)$$

$$(\mathcal{A}_s)_{\bar{e}\bar{\mu}} = [0.98(a_L)_{\bar{e}\bar{\mu}}^X + 0.053(a_L)_{\bar{e}\bar{\mu}}^Y] + E[-1.96(c_L)_{\bar{e}\bar{\mu}}^{TX} - 0.11(c_L)_{\bar{e}\bar{\mu}}^{TY} - 0.38(c_L)_{\bar{e}\bar{\mu}}^{XZ} - 0.021(c_L)_{\bar{e}\bar{\mu}}^{YZ}], \quad (10)$$

$$(\mathcal{A}_c)_{\bar{e}\bar{\mu}} = [0.053(a_L)_{\bar{e}\bar{\mu}}^X - 0.98(a_L)_{\bar{e}\bar{\mu}}^Y] + E[-0.11(c_L)_{\bar{e}\bar{\mu}}^{TX} + 1.96(c_L)_{\bar{e}\bar{\mu}}^{TY} - 0.021(c_L)_{\bar{e}\bar{\mu}}^{XZ} + 0.38(c_L)_{\bar{e}\bar{\mu}}^{YZ}], \quad (11)$$

$$(\mathcal{B}_s)_{\bar{e}\bar{\mu}} = E[-0.052((c_L)_{\bar{e}\bar{\mu}}^{XX} - (c_L)_{\bar{e}\bar{\mu}}^{YY}) + 0.96(c_L)_{\bar{e}\bar{\mu}}^{XY}], \quad (12)$$

$$(\mathcal{B}_c)_{\bar{e}\bar{\mu}} = E[0.48((c_L)_{\bar{e}\bar{\mu}}^{XX} - (c_L)_{\bar{e}\bar{\mu}}^{YY}) + 0.10(c_L)_{\bar{e}\bar{\mu}}^{XY}]. \quad (13)$$

In Eq. 9, the mass-squared term, $\tilde{m}_{\bar{e}\bar{\mu}}^2$, has been included. This allows for conventional massive-neutrino oscillations in addition to the Lorentz-violation oscillations. It is assumed that the size of this term does not invalidate the short-baseline approximation [29].

V. SIDEREAL TIME DISTRIBUTION OF THE LSND DATA

In conventional explanations of neutrino oscillations, the oscillation probability is independent of sidereal time and, therefore, the sidereal time distribution of oscillation events is expected to be constant. In the Lorentz and CPT violating model of neutrino oscillations considered here, nonzero values of the model parameters could exhibit themselves as modulations to the sidereal time distribution (as in Eq. 7). The sidereal time dependence of candidate oscillation events from the LSND data sample has been examined and subjected to statistical tests to quantify any evidence for a sidereal variation.

In the analysis of the final LSND data set [14], 205 neutrino oscillation candidate events were reported with positron energy in the range $20 < E_e < 60$ MeV and with an identified neutron-capture photon. There are two

classes of background in the oscillation sample: beam-unrelated and beam-related (ν -induced). The beam-unrelated backgrounds arise from cosmic ray processes. It is measured in beam-off data and then subtracted from the beam-on data. The beam-related backgrounds are calculated from known neutrino (nonoscillation) interactions.

The neutrino beam used for the LSND experiment was produced using protons from the LANSCE accelerator [32]. The proton beam was delivered at approximately 100Hz in pulses of 600 μ s duration. The detector was triggered independently of the state of the beam and the beam status was recorded. In this manner, beam-off data was taken continuously in the time between beam pulses. The resulting beam-off data set was approximately 16 times larger than the beam-on data set. This allowed for an accurate measurement of the beam-unrelated background by weighting the beam-off data by the beam duty-factor (calculated for each run).

The estimated number of beam-unrelated and ν -induced background events in this sample are 106.8 ± 2.5 and 39.2 ± 3.1 , respectively. These events were collected during experimental running in 1993 through 1998. There were six sets of runs, one in each of these years. The GPS (Global Positioning System) time stamp, necessary for this analysis, was not included into the LSND data stream until midway through the 1994 run period. Because of this, only 186 of the 205 oscillation candidate events could be used in this analysis. The expected numbers of beam-off and ν -induced backgrounds in this smaller sample are 94.0 ± 2.3 and 35.6 ± 2.8 , respectively.

Ideally, an experiment to search for sidereal variations in a signal would run continuously throughout the calendar year so that one particular sidereal time bin would be drawn from the entire range of local time. This was not the case with LSND, but runs did cover the space of local time vs sidereal time with reasonable completeness, as can be seen in Figure 2. The Los Alamos (clock) time can be determined from Greenwich Mean (GM) time by subtracting 6 (7) hours in the summer (winter).

To quantify the statistical significance of any sidereal time variation in the data, we employed two different statistical tests: a Pearson's- χ^2 test [33, 34] and a Kolmogorov-Smirnov (KS) test [34]. In both of these tests, the data were compared to the (null) hypothesis that the event rate is constant in sidereal time. Note that this null hypothesis is not that no oscillation signal exists, but only that the signal is constant in time. We also examined the GM time distributions and applied these tests with the null hypothesis of an underlying distribution that is constant in GM time.

The Pearson's- χ^2 ($P-\chi^2$), as implemented in this analysis, is

$$P-\chi^2 = \sum_{i=1}^N \frac{(n_i - \nu_i)^2}{\nu_i}; \nu_i = n/N, \quad (14)$$

where n is the total number of events in the sample, N is the number of time bins, and n_i is the measured number

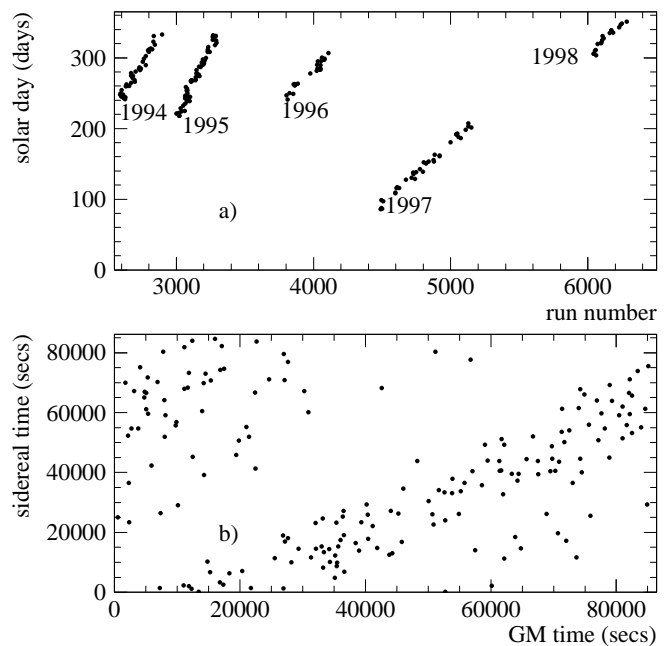


FIG. 2: Distribution of beam-on neutrino candidate events in a) run number vs. solar day (day 1= January 1) and b) GM time vs sidereal time. The year of each set of runs is indicated in a).

of events in time bin i . The predicted number of events in each time bin, ν_i , is constant for each time bin. Note that this quantity is constructed with the variance of the *expected* number of events in the denominator.

The $P-\chi^2$ statistic will follow, in the absence of sidereal time variations and with sufficient events per time bin, a χ^2 distribution with number of degrees of freedom equal to the number of time bins minus one [33, 34]. The standard criterion for sufficient events is that $\nu_i \geq 5$ [33, 34]. The binning for the beam-on data has been chosen to satisfy this. The p -value, ($P(\chi^2)$, one minus the χ^2 cumulative distribution) can be extracted and interpreted as a confidence level that the null hypothesis explains the data.

The KS test has the advantage that it works with unbinned data, thus eliminating the need to choose a binning. It involves a comparison between the data and the null hypothesis via cumulative distributions. Unlike the $P-\chi^2$ test, it is sensitive to “runs” in the data, thus making the $P-\chi^2$ and KS tests complementary. The KS statistics reported here are the maximum cumulative deviation, D_n , and the KS probability, $P(\text{KS})$. The quantity $P(\text{KS})$, which is obtained from the known distribution of D_n [34], can be interpreted as a confidence level that the data is explained by the null hypothesis.

In the LSND data set considered for this analysis, there were 1656 beam-off events passing the neutrino oscillation cuts. These events, after weighting for the beam-on duty-factor, determine the number and distributions of beam-unrelated background events in the beam-on sam-

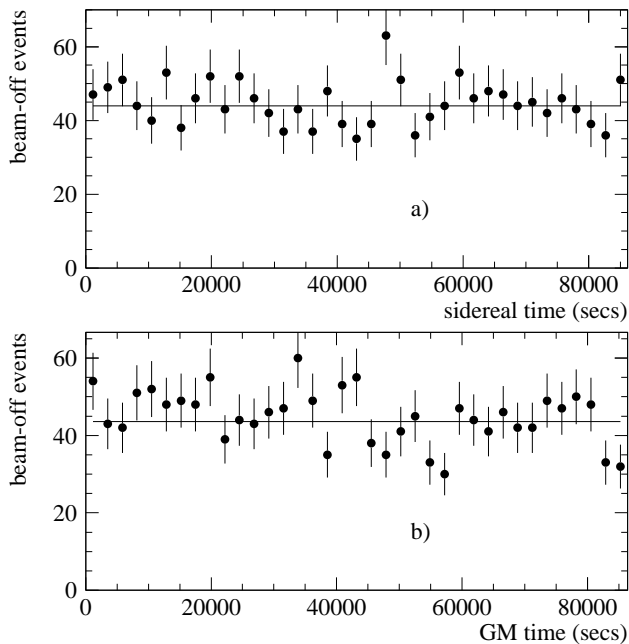


FIG. 3: Sidereal a) and GM b) time distributions of beam-off data using 37 time bins. The solid lines indicate the expected underlying distribution with no sidereal time variation. The errors bars displayed in this plot (and subsequent) are the square root of the number in each bin.

ple. The distribution of sidereal and GM times in 37 time bins for these beam-off events is shown in Fig. 3. The number of time bins chosen for this distribution was obtained by applying the $N > 5$ criterion for the beam-on data. The errors shown in Fig. 3 (and subsequent figures) are the square root of the number of counts in the bin. Note that these errors are not used in the calculation of the $P\text{-}\chi^2$ (Eq. 14). The $P\text{-}\chi^2$ is 29.6 for 37 sidereal time bins corresponding to $P(\chi^2) = 0.77$. The KS test on this same data yields $D_n = 0.019$ and $P(\text{KS}) = 0.60$. These results indicate that the beam-off data are in reasonable agreement with the null hypothesis (no sidereal time dependence). The GM time distribution yields a slightly low $P(\text{KS}) = 0.01$, however, for this same distribution $P(\chi^2) = 0.29$. In addition, any GM time variations are distributed throughout a range in sidereal time. For these reasons, we conclude that there is no evidence for substantial environmental or “day-night” sidereal variations in the beam-unrelated backgrounds.

The sidereal and GM time distributions of the 186 oscillation candidate events are shown in Figure 4. The $P\text{-}\chi^2$ for the sidereal time distributions is 44.8 for 37 time bins. The corresponding p -value for the sidereal time distribution is $P(\chi^2) = 0.15$. A KS test applied to these distributions yields $P(\text{KS}) = 0.234$. The sidereal time distribution is slightly less compatible with no time variation as is evident in both of these statistical tests. However, the variation is not statistically significant. A KS test between beam-on and beam-off data was also

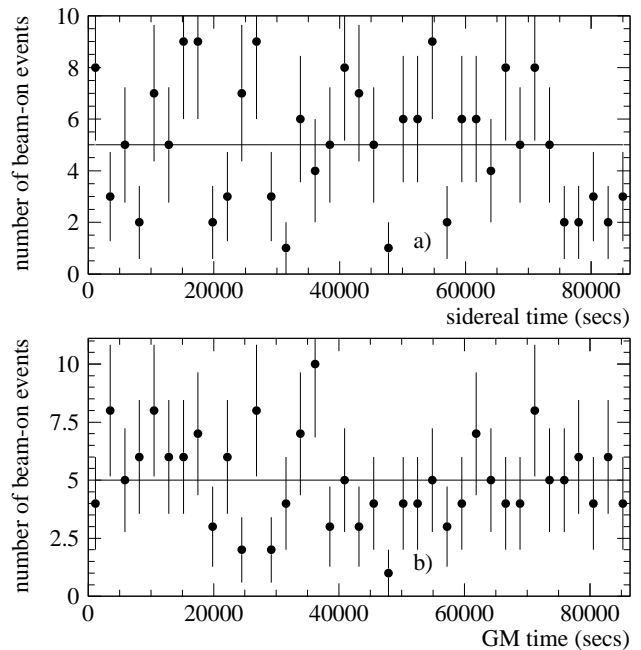


FIG. 4: Sidereal a) and GM b) time distributions of the 186 beam-on oscillation candidate events in 37 bins. The solid lines indicate the expected underlying distribution with no sidereal time variation.

applied and shows compatibility between the two data sets. The complete results from the statistical tests on the sidereal and GM time distributions for beam-on and beam-off data are summarized in Table I.

To check the underlying assumption that the beam was delivered with equal efficiency throughout the sidereal day, a sample of $^{12}\text{C}(\nu_e, e^-)^{12}\text{N}_{\text{g.s.}}$ events was obtained by applying cuts to select for subsequent β -decays of $^{12}\text{N}_{\text{g.s.}}$ (as described in Ref. [35]). This procedure yields 722 beam-on events with a beam-unrelated background of 17.5 events. The sidereal time distribution of these beam-on events are shown in Fig. 5. The $P\text{-}\chi^2$ for this sidereal time distributions is 29.3 for 37 time bins which corresponds to $P(\chi^2) = 0.78$. The Kolmogorov-Smirnov test yields $D_n = 0.020$ and $P(\text{KS}) = 0.94$. The values indicate that the assumption of constant beam delivery, averaged over the sidereal day and over all LSND runs, is consistent with the data.

VI. THE EXTRACTION OF THE SME PARAMETERS

While the LSND oscillation data examined in the previous section shows no statistically significant sidereal time variation, it is interesting to examine the data in context of the SME model explained in Section IV. First, this model does not require a sidereal time variation and, second, the LSND data set does allow for some sidereal time variation.

null hypothesis tests				
	beam-on		beam-off	
	sidereal	GM	sidereal	GM
# of events	186		1656	
Pearson's χ^2:				
N_{bins}	37	37	37	37
χ^2	44.8	27.6	29.6	40.3
$P(\chi^2)$	0.15	0.84	0.77	0.29
Kolmogorov-Smirnov:				
D_n	0.076	0.066	0.019	0.040
$P(\text{KS})$	0.234	0.386	0.604	0.010

beam-on/beam-off tests		
	sidereal	GM
D_n	0.067	0.046
$P(\text{KS})$	0.432	0.864

TABLE I: A summary of results from statistical tests on the sidereal and GM time distributions of the $20 < E_{e^+} < 60$ MeV neutrino oscillation data. The null hypothesis tests compare the data with a constant time distribution. The beam-on/beam-off tests compare the two sets.

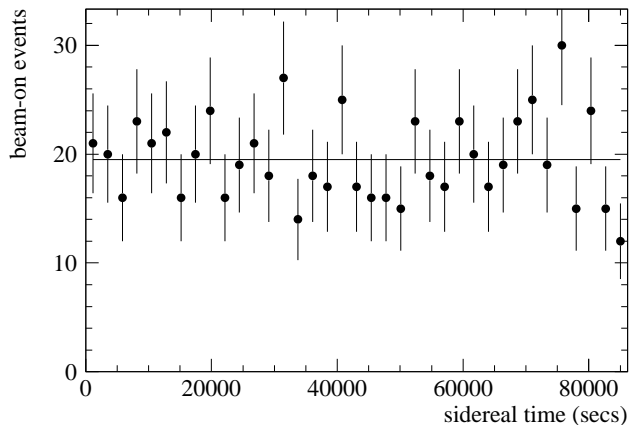


FIG. 5: Sidereal time distribution of beam-on data with $^{12}\text{C}(\nu_e, e^-)^{12}\text{N}_{\text{g.s.}}$ cuts. The line indicates the average value.

A maximum-likelihood method, with Eq. 7 as a description of the oscillation signal, was performed to extract allowed values of the SME parameters, $(\mathcal{C})_{\bar{e}\bar{\mu}}$, $(\mathcal{A}_s)_{\bar{e}\bar{\mu}}$, $(\mathcal{A}_c)_{\bar{e}\bar{\mu}}$, $(\mathcal{B}_s)_{\bar{e}\bar{\mu}}$, and $(\mathcal{B}_c)_{\bar{e}\bar{\mu}}$. In general, these parameters are complex — the special case is considered here where these parameters are real. Also, the values extracted are an effective average over the energy range of the LSND data set, $20 < E_{e^+} < 60$ MeV.

The parameters were extracted using an unbinned likelihood function,

$$\Lambda = \frac{e^{-\mu}}{N!} \prod_{i=1}^N (\mu_s \mathcal{F}_s + \mu_b \mathcal{F}_b)$$

$$\times \prod_{i=s,b} \frac{1}{\sqrt{2\pi}\sigma_i^2} \exp\left(-\frac{(\mu_i - \bar{\mu}_i)^2}{2\sigma_i^2}\right) \quad (15)$$

where N is the total number of events in the sample, μ_s is the total predicted oscillation signal events, μ_b is the estimated number of background events, and $\mu = \mu_s + \mu_b$. The shape of the data in sidereal time is described with the functions \mathcal{F}_s and \mathcal{F}_b . \mathcal{F}_s depends on the SME parameters as in Eq. 7 and \mathcal{F}_b is assumed to be constant in sidereal time. The latter half of the likelihood function describes systematic errors on the signal and background events. In implementation, the natural log of the likelihood function, $\ell (= \ln \Lambda)$, was used. Note that this function describes both the shape and the overall number of events.

Three different parameter combinations were considered.

- **1-parameter:**

$$(\mathcal{C})_{\bar{e}\bar{\mu}} \neq 0; (\mathcal{A}_s)_{\bar{e}\bar{\mu}}, (\mathcal{A}_c)_{\bar{e}\bar{\mu}}, (\mathcal{B}_s)_{\bar{e}\bar{\mu}}, (\mathcal{B}_c)_{\bar{e}\bar{\mu}} = 0$$

The “rotationally invariant” case [36, 37, 38, 39].

- **3-parameter:**

$$(\mathcal{C})_{\bar{e}\bar{\mu}}, (\mathcal{A}_s)_{\bar{e}\bar{\mu}}, (\mathcal{A}_c)_{\bar{e}\bar{\mu}} \neq 0; (\mathcal{B}_s)_{\bar{e}\bar{\mu}}, (\mathcal{B}_c)_{\bar{e}\bar{\mu}} = 0$$

Includes all of the CPT-odd terms of the minimal-SME model.

- **5-parameter:**

$$(\mathcal{C})_{\bar{e}\bar{\mu}}, (\mathcal{A}_s)_{\bar{e}\bar{\mu}}, (\mathcal{A}_c)_{\bar{e}\bar{\mu}}, (\mathcal{B}_s)_{\bar{e}\bar{\mu}}, (\mathcal{B}_c)_{\bar{e}\bar{\mu}} \neq 0$$

Full minimal-SME model including both CPT-odd and CPT-even terms.

Using each of these three parameter sets, the log likelihood, ℓ , was calculated for the 186 candidate oscillation events as each of the parameters in the set was varied in a range around zero. The sidereal time for the parameter values that maximized ℓ is plotted together with the data in Figure 6. Note that the data in Fig. 6 is grouped into 24 time bins instead of 37 as was used in Fig. 4. This is to allow for the quality of the fit to be more easily seen.

The maximum- ℓ solutions are summarized below. The likelihood contours for the 3-parameter combination are shown in Fig. 7. The (1σ) errors were calculated by determining the parameter ranges where ℓ decreased by 0.5 (1-parameter), 1.77 (3-parameters), or 3.0 (5-parameters) from the maximum value.

- **1-parameter:**

$$(\mathcal{C})_{\bar{e}\bar{\mu}} = 3.3 \pm 0.4 \pm 0.2 \quad (16)$$

- **3-parameter:**

There are two solutions within the 1σ likelihood region (see Fig. 7).

Solution 1 (maximum- ℓ):

$$\begin{aligned} (\mathcal{C})_{\bar{e}\bar{\mu}} &= -0.2 \pm 1.0 \pm 0.3, \\ (\mathcal{A}_s)_{\bar{e}\bar{\mu}} &= 4.0 \pm 1.3 \pm 0.4, \\ (\mathcal{A}_c)_{\bar{e}\bar{\mu}} &= 1.9 \pm 1.8 \pm 0.4. \end{aligned} \quad (17)$$

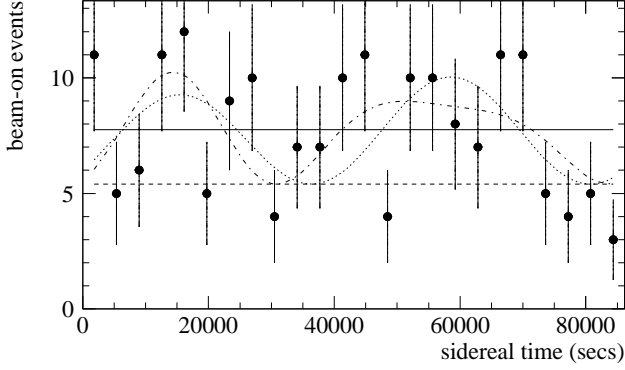


FIG. 6: Sidereal time distribution of the LSND oscillation data in 24 time bins together with the maximum- ℓ solutions for the 1-parameter (solid line), 3-parameter (dotted), and 5-parameter (dot-dashed) combinations. The dashed line indicates the estimated background contribution.

Solution 2:

$$\begin{aligned} (\mathcal{C})_{\bar{e}\bar{\mu}} &= 3.3 \pm 0.5 \pm 0.3, \\ (\mathcal{A}_s)_{\bar{e}\bar{\mu}} &= 0.1 \pm 0.6 \pm 0.2, \\ (\mathcal{A}_c)_{\bar{e}\bar{\mu}} &= -0.5 \pm 0.6 \pm 0.2. \end{aligned} \quad (18)$$

- **5-parameter:** Multiple (connected) solutions exist in the 5-parameter case making a numerical extraction of errors impossible. The maximum- ℓ solution is:

$$\begin{aligned} (\mathcal{C})_{\bar{e}\bar{\mu}} &= -0.7, \\ (\mathcal{A}_s)_{\bar{e}\bar{\mu}} &= 3.7, \\ (\mathcal{A}_c)_{\bar{e}\bar{\mu}} &= 2.3, \\ (\mathcal{B}_s)_{\bar{e}\bar{\mu}} &= 0.9, \\ (\mathcal{B}_c)_{\bar{e}\bar{\mu}} &= -0.6. \end{aligned} \quad (19)$$

All parameters have units of 10^{-19} GeV and the errors quoted above are in the form $\pm(\text{statistical})\pm(\text{systematic})$.

In all of these results, duplicate solutions exist with opposite signs for all of the parameters. Note that in the 3-parameter case, the two solutions correspond to a large value for $(\mathcal{C})_{\bar{e}\bar{\mu}}$ with a small value for $(\mathcal{A}_s)_{\bar{e}\bar{\mu}}$, $(\mathcal{A}_c)_{\bar{e}\bar{\mu}}$ and *vice versa*. The small- $(\mathcal{C})_{\bar{e}\bar{\mu}}$, large- $(\mathcal{A}_s)_{\bar{e}\bar{\mu}}$, $(\mathcal{A}_c)_{\bar{e}\bar{\mu}}$ solution is only slightly favored over the large- $(\mathcal{C})_{\bar{e}\bar{\mu}}$, small- $(\mathcal{A}_s)_{\bar{e}\bar{\mu}}$, $(\mathcal{A}_c)_{\bar{e}\bar{\mu}}$ solution. This is because the sinusoidal terms in Eq. 7 improve the description of the data in sidereal time, although, an oscillation probability that is constant in sidereal time is consistent with the data (as was reported in Sec. V). Note also that the solution where $(\mathcal{C})_{\bar{e}\bar{\mu}}$ is the only nonzero term can be identified with the conventional neutrino oscillation description via the first term of Eq. 9. A solution with all parameters ≈ 0 is highly disfavored. This is equivalent to the statement that the LSND oscillation excess is statistically significant.

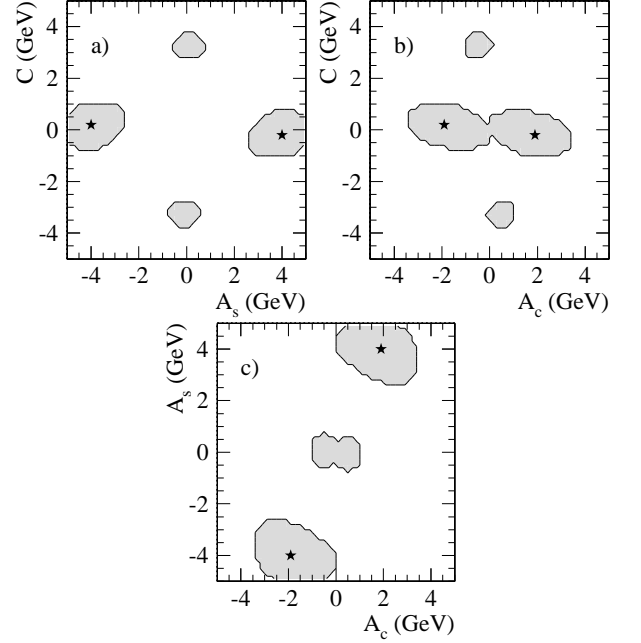


FIG. 7: Log likelihood values for the 3-parameter description of the LSND sidereal time distribution: a) $(\mathcal{A}_s)_{\bar{e}\bar{\mu}}$ vs $(\mathcal{C})_{\bar{e}\bar{\mu}}$, b) $(\mathcal{A}_c)_{\bar{e}\bar{\mu}}$ vs $(\mathcal{C})_{\bar{e}\bar{\mu}}$, and c) $(\mathcal{A}_c)_{\bar{e}\bar{\mu}}$ vs $(\mathcal{A}_s)_{\bar{e}\bar{\mu}}$. The contours in a)-c) indicate the 1- σ (total error) allowed regions ($\ell > \ell_{\text{max}} - 1.77$) and the stars indicate the maximum- ℓ parameter values.

Since the oscillation probability depends on the SME parameters *squared*, the results for the SME parameters obtained above are more easily compared to the measured oscillation probability from LSND via combinations of the squares of the parameters. The value resulting from the 1-parameter solution is

$$|(\mathcal{C})_{\bar{e}\bar{\mu}}|^2 = 10.7 \pm 2.6 \pm 1.3 (10^{-19}\text{GeV})^2. \quad (20)$$

The values for the parameter square sum resulting from the multiparameter combinations are more highly constrained than for individual parameters. The value extracted from the 3-parameter solution is

$$\begin{aligned} |(\mathcal{C})_{\bar{e}\bar{\mu}}|^2 + \frac{1}{2}|(\mathcal{A}_s)_{\bar{e}\bar{\mu}}|^2 + \frac{1}{2}|(\mathcal{A}_c)_{\bar{e}\bar{\mu}}|^2 \\ = 9.9 \pm 2.3 \pm 1.4 (10^{-19}\text{GeV})^2, \end{aligned} \quad (21)$$

and from the 5-parameter solution,

$$\begin{aligned} |(\mathcal{C})_{\bar{e}\bar{\mu}}|^2 + \frac{1}{2}|(\mathcal{A}_s)_{\bar{e}\bar{\mu}}|^2 + \frac{1}{2}|(\mathcal{A}_c)_{\bar{e}\bar{\mu}}|^2 \\ + \frac{1}{2}|(\mathcal{B}_s)_{\bar{e}\bar{\mu}}|^2 + \frac{1}{2}|(\mathcal{B}_c)_{\bar{e}\bar{\mu}}|^2 \\ = 10.5 \pm 2.4 \pm 1.4 (10^{-19}\text{GeV})^2. \end{aligned} \quad (22)$$

These results for the combination of SME parameters are consistent with the previously reported oscillation probability from LSND [14] and with the estimate presented in Ref. [29].

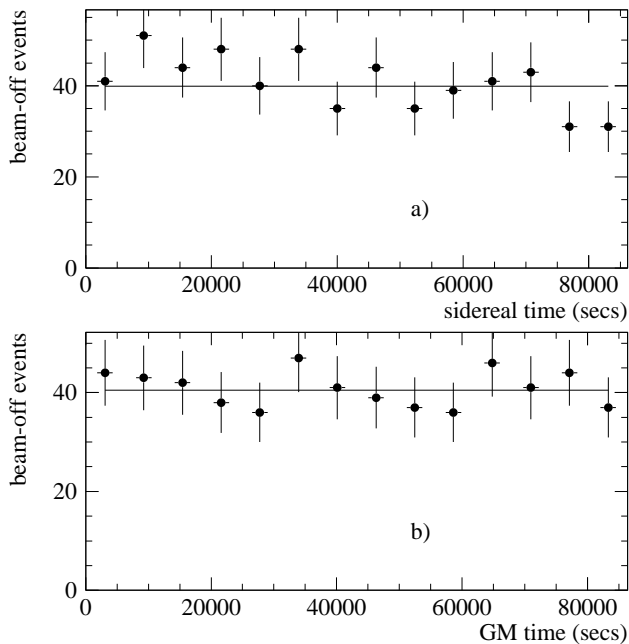


FIG. 8: Sidereal a) and GM b) time distributions of the high-energy, beam-off data in 14 bins. The solid lines indicate the expected underlying distribution with no sidereal time variation.

VII. A HIGH-ENERGY SUBSET OF THE LSND DATA

A high-energy subset of the LSND data with a positron energy cut, $36 < E_{e^+} < 60$ MeV, is interesting to examine separately. The ν -induced background is reduced in this sample [14]. Furthermore, the $1/E$ prefactor to the mass term in Eq. 9 would suppress the conventional oscillation terms relative to any Lorentz-violation terms present.

This reduced data set consists of 73 beam-on events with expected beam-unrelated and ν -induced background events of 31.3 ± 0.8 and 10.0 ± 0.8 , respectively. The sidereal and GM time distributions of the 571 beam-off events passing these high-energy cuts are shown in Figure 8. The $P\text{-}\chi^2$ is 12.2 for 14 sidereal time bins, corresponding to $P(\chi^2) = 0.51$. The resulting p -value from the KS test to this distribution is $P(\text{KS}) = 0.080$. Again, these values show no reason to reject the null hypothesis for beam-off data.

The sidereal time distribution of the high-energy beam-on data is shown in Figure 9. The $P\text{-}\chi^2$ is 20.4 for 14 sidereal time bins corresponding to $P(\chi^2) = 0.09$. The resulting p -value for the KS test is $P(\text{KS}) = 0.178$. Although these values indicate a slightly reduced agreement with the null hypothesis, they do not indicate a statistically significant sidereal variation. The complete results from the statistical tests on the sidereal and GM time distributions for the high-energy data are summarized in Table II.

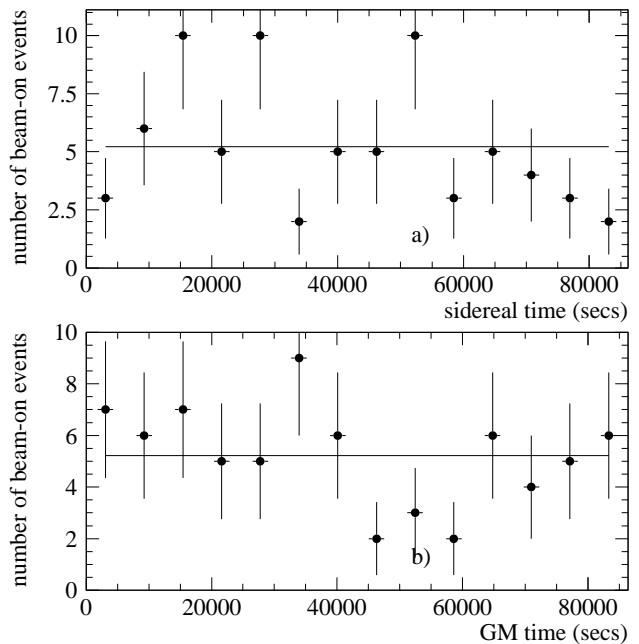


FIG. 9: Sidereal a) and GM b) time distributions of the 73 LSND high-energy, beam-on oscillation candidate events in 14 bins. The solid lines indicate the expected underlying distribution with no sidereal time variation.

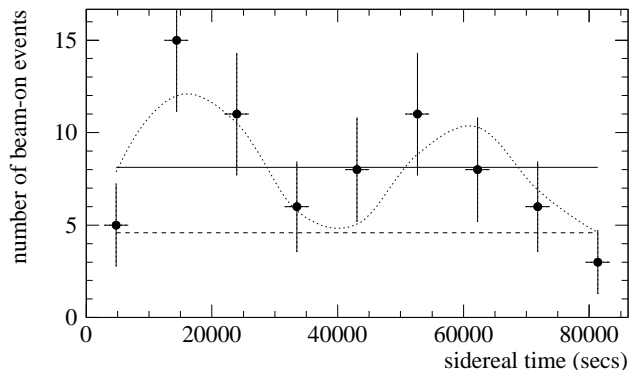


FIG. 10: Sidereal time distribution of the high-energy LSND oscillation data in 9 time bins together with the maximum- ℓ solutions for the 1-parameter (solid line) and 3-parameter (dotted) combinations. The dashed line indicates the estimated background contribution.

The maximum-likelihood procedure was applied to this high-energy data set using the 1- and 3-parameter combinations described in Section VI. The limited data sample did not allow for the 5-parameter combination. Figure 10 (with a reduced bin size) shows 1- and 3-parameter maximum- ℓ solutions superimposed on the high-energy data. Both parameter combinations produce acceptable descriptions of the data.

The values for the parameter square sums extracted with the maximum-likelihood method are summarized below. The likelihood contours for the 3-parameter com-

null hypothesis tests				
	beam-on		beam-off	
	sidereal	GM	sidereal	GM
# of events	73		571	
Pearson's χ^2 :				
N_{bins}	14	14	14	14
χ^2	20.4	9.7	12.2	4.4
$P(\chi^2)$	0.09	0.72	0.51	0.99
Kolmogorov-Smirnov:				
D_n	0.129	0.123	0.053	0.026
$P(\text{KS})$	0.178	0.221	0.080	0.826

beam-on/beam-off tests		
	sidereal	GM
D_n	0.094	0.107
$P(\text{KS})$	0.621	0.451

TABLE II: A summary of results from statistical tests on the sidereal and GM time distributions of the LSND $36 < E_{e^+} < 60$ MeV neutrino oscillation data. These values result from the same procedure as used for Table I.

bination are shown in Fig. 11.

- **1-parameter:**

$$|(\mathcal{C})_{\bar{e}\bar{\mu}}|^2 = 10.7 \pm 2.9 \pm 1.5 (10^{-19}\text{GeV})^2 \quad (23)$$

- **3-parameter:**

$$\begin{aligned} |(\mathcal{C})_{\bar{e}\bar{\mu}}|^2 + \frac{1}{2}|(\mathcal{A}_s)_{\bar{e}\bar{\mu}}|^2 + \frac{1}{2}|(\mathcal{A}_c)_{\bar{e}\bar{\mu}}|^2 \\ = 10.2 \pm 2.7 \pm 1.3 (10^{-19}\text{GeV})^2 \end{aligned} \quad (24)$$

As can be seen by comparing the results from the high-energy subset with the entire data set, there are no significant differences. The time distributions from the high-energy subset are consistent with no sidereal variation and the results from the SME-parameter extraction are consistent with those obtained from the entire data set.

VIII. A GLOBAL SOLUTION OF NEUTRINO OSCILLATIONS?

To determine the implications of the allowed SME-parameter values extracted from the LSND data, consider the situation where the only nonzero term is $(\mathcal{A}_s)_{\bar{e}\bar{\mu}}$. This term was the largest in the maximum- ℓ solutions that allowed for sidereal variation. In this case, one or more of the SME coefficients, $(a_L)_{\bar{e}\bar{\mu}}^X$, $(a_L)_{\bar{e}\bar{\mu}}^Y$, $(c_L)_{\bar{e}\bar{\mu}}^{TX}$, $(c_L)_{\bar{e}\bar{\mu}}^{TY}$, $(c_L)_{\bar{e}\bar{\mu}}^{XZ}$ and $(c_L)_{\bar{e}\bar{\mu}}^{YZ}$ would be nonzero (as can be seen from Eq. 10).

A simple interpretation is that one of the a_L -type SME coefficients is of order 10^{-19} GeV or one of the c_L -type

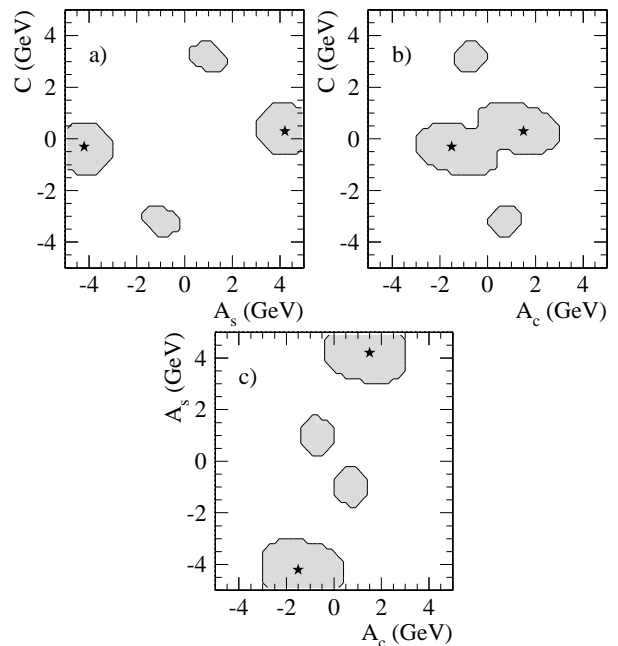


FIG. 11: Log likelihood values for the 3-parameter description of the high-energy LSND sidereal time distribution: a) $(\mathcal{A}_s)_{\bar{e}\bar{\mu}}$ vs $(\mathcal{C})_{\bar{e}\bar{\mu}}$, b) $(\mathcal{A}_c)_{\bar{e}\bar{\mu}}$ vs $(\mathcal{C})_{\bar{e}\bar{\mu}}$, and c) $(\mathcal{A}_s)_{\bar{e}\bar{\mu}}$ vs $(\mathcal{A}_c)_{\bar{e}\bar{\mu}}$. The contours in a)-c) indicate the $1\text{-}\sigma$ (total error) allowed regions ($\ell > \ell_{\text{max}} - 1.77$) and the stars indicate the maximum- ℓ parameter values.

is of order 10^{-17} (or $E \times c_L \sim 10^{-19}$ GeV, where E is the neutrino energy). These values would have significant implications in other neutrino oscillation experiments and produce effects that have not been observed. In the simplest class of models, the acceptable maximum scale of Lorentz and CPT violation for reactor neutrino oscillations is $a_L \sim 10^{-21}$ GeV, $c_L \sim 10^{-22}$, and, for long-baseline neutrino oscillations, $a_L \sim 10^{-22}$ GeV, $c_L \sim 10^{-19}$ [13, 36, 37, 38, 39]. However, there is no theoretical motivation that nature has chosen a simple solution for neutrino oscillations [40]. A global solution of neutrino oscillations with Lorentz and CPT violation that accommodates all the data may yet be obtainable within this SME framework.

For this reason, it is important to search for sidereal variations in other short-baseline neutrino oscillation experiments. The data can be analyzed with the same method as presented here.

The currently running MiniBooNE experiment [27], with a different beam energy and with a ν_μ beam, will be able to test these LSND solutions for Lorentz and CPT violating neutrino oscillations with a high-statistics appearance measurement. In particular, a measurement from MiniBooNE would provide an additional five constraints (Eqs. 9-13) on the SME coefficients. The neutrino propagation vectors are different for MiniBooNE as the neutrino beamline is oriented toward compass north (as opposed to east for LSND). Also, the SME coeffi-

cients would be transformed for the neutrino case [29]. If MiniBooNE collects a significant set of data with a $\bar{\nu}_\mu$ beam, an additional set of constraints with antineutrino coefficients would also be obtained.

Of course, results from other neutrino oscillation experiments would add further valuable information. This has been investigated for Super-Kamiokande [41] and MINOS [42].

IX. CONCLUSIONS

The neutrino oscillation candidate events from the LSND experiment have been examined for evidence of sidereal time variation — a possible signal for Lorentz violation in the neutrino sector. The oscillation excess is consistent with no sidereal time variation. An examination of a high-energy subset of the data yields the same conclusion.

A “smoking-gun” for Lorentz violation has not been found in the LSND signal. However, the data are ad-

equately described within the SME neutrino oscillation formalism that includes both Lorentz and CPT violation [13, 29]. A maximum-likelihood method was used to determine allowed parameter regions for SME parameter combinations. They indicate values on the order of 10^{-19} GeV for a_L and $E \times c_L$. These values are in the range expected for Planck-scale effects in the neutrino sector. Future results from high-statistics oscillation experiments will allow more stringent tests of the SME framework.

X. ACKNOWLEDGMENTS

This work was conducted under the auspices of the US Department of Energy, supported in part by funds provided by the University of California for the conduct of discretionary research by Los Alamos National Laboratory. This work was also supported by the National Science Foundation.

-
- [1] V. A. Kostelecky and S. Samuel, Phys. Rev. D **39**, 683 (1989).
- [2] S. W. Hawking, Phys. Rev. D **14**, 2460 (1976).
- [3] V. A. Kostelecký ed., *CPT and Lorentz Symmetry III* (World Scientific, Singapore, 2005).
- [4] D. Colladay and V.A. Kostelecký, Phys. Rev. D **55**, 6760 (1997); Phys. Rev. D **58**, 116002 (1998); V. A. Kostelecky, Phys. Rev. D **69**, 105009 (2004).
- [5] F. Canè *et al.*, Phys. Rev. Lett. **93**, 230801 (2004).
- [6] V. A. Kostelecky and M. Mewes, Phys. Rev. Lett. **87**, 251304 (2001); Phys. Rev. D **66**, 056005 (2002).
- [7] V.A. Kostelecký, Phys. Rev. Lett. **80**, 1818 (1998); Phys. Rev. D **64**, 076001 (2001); Phys. Rev. D **61**, 016002 (2000).
- [8] Y.B. Hsiung *et al.* [KTeV collaboration] Nucl. Phys. Proc. Suppl. **86**, 312 (2000).
- [9] J. Link *et al.* [FOCUS collaboration] Phys. Lett. B **556**, 7 (2003); A. Kryemadhi, Ph.D. dissertation, Indiana University (2004).
- [10] B. Aubert *et al.* [BaBar collaboration] [arXiv:hep-ex/0303043].
- [11] K. Abe *et al.* [BELLE collaboration] Phys. Rev. Lett. **86**, 3228 (2001).
- [12] R. Akerstaff *et al.* [OPAL collaboration] Z. Phys. C **76**, 401 (1997).
- [13] V.A. Kostelecký and M. Mewes, Phys. Rev. D **69**, 016005 (2004).
- [14] A.A. Aguilar *et al.* [LSND Collaboration], Phys. Rev. D **64**, 112007 (2001).
- [15] B.T. Cleveland *et al.* [Homestake Collaboration], Ap. J. **496**, 505 (1998).
- [16] K.S. Hirata *et al.* [Kamiokande Collaboration], Phys. Rev. Lett. **63** 16 (1989).
- [17] W. Hampel *et al.* [GALLEX Collaboration], Phys. Lett. B **447**, 127 (1999).
- [18] J.N. Abdurashitov *et al.* [SAGE collaboration], J. Exp. Theor. Phys. **95** 181 (2002).
- [19] M. Altmann *et al.* [GNO Collaboration], Phys. Lett. B **490**, 16 (2000).
- [20] Q.R. Ahmad *et al.* [SNO Collaboration], Phys. Rev. Lett. **87**, 071301 (2001).
- [21] Y. Fukuda *et al.* [Super-Kamiokande Collaboration] Phys. Rev. Lett. **81**, 1562 (1998).
- [22] M. Ambrosio *et al.* [MACRO Collaboration] Phys. Lett. B **566**, 35 (2003).
- [23] M.H. Ahn *et al.* [K2K Collaboration] Phys. Rev. Lett. **90**, 041801 (2003).
- [24] K. Eguchi *et al.* [KamLAND Collaboration] Phys. Lett. **90**, 021802 (2003).
- [25] G. Barenboim *et al.*, Phys. Lett. B **537**, 227 (2002).
- [26] M. Sorel, J. M. Conrad and M. Shaevitz, Phys. Rev. D **70**, 073004 (2004).
- [27] R. Tayloe [MiniBooNE Collaboration], Nucl. Phys. Proc. Suppl. **118**, 157 (2003); E. Church *et al.*, FERMILAB-PROPOSAL-0898.
- [28] T. Katori and R. Tayloe, in Ref. [3].
- [29] V.A. Kostelecký and M. Mewes, Phys. Rev. D **70**, 076002 (2004).
- [30] R. Bluhm *et al.*, Phys. Rev. D **68**, 125008 (2003).
- [31] <http://www.teraserver.com/imagery/>.
- [32] C. Athanassopoulos *et al.* [LSND Collaboration], Nucl. Instrum. Meth. A **388**, 149 (1997).
- [33] S. Eidelman *et al.* [Particle Data Group Collaboration], Phys. Lett. B **592**, 1 (2004).
- [34] A. Frodesen, O. Skjeggstad, and H. Tøfte, *Probability and Statistics in Particle Physics*, (Universitetsforlaget, Bergen, 1979).
- [35] L. B. Auerbach *et al.* [LSND Collaboration], Phys. Rev. C **64**, 065501 (2001).
- [36] S. Coleman and S.L. Glashow, Phys. Rev. D **59**, 116008 (1999).
- [37] V. Barger *et al.*, Phys. Rev. Lett. **85**, 5055 (2000).

- [38] J.N. Bahcall, V. Barger, and D. Marfatia, Phys. Lett. B **534**, 120 (2002).
- [39] J.N. Bahcall, M.C. Gonzalez-Garcia, and C. Peña-Garay, JHEP **0408**, 016 (2004).
- [40] V. A. Kostelecky and M. Mewes, Phys. Rev. D **70**, 031902 (2004).
- [41] M. D. Messier, in Ref. [3].
- [42] B. J. Rebel and S. L. Mufson in Ref. [3].